Bounding Surface Constitutive Model for Cemented Sand under Monotonic Loading

Mojtaba Rahimi, Ph.D.[1]; Dave Chan, Ph.D., P.Eng.[2]; and Alireza Nouri, Ph.D., P.Eng.[3]

Abstract: This paper presents a critical state constitutive model for cemented sand. The model uses a single capped yield surface as a function of the void ratio, confining pressure, preconsolidation pressure, and stress ratio at the peak of the undrained effective stress path. To model the cemented materials, the formulation of the yield function, elastic moduli, plastic modulus, flow rule, and other components of the model have been modified. Having incorporated the tensile strength and cohesion, the radial-mapping formulation of the bounding surface plasticity is incorporated in the model. The modified model has been calibrated and verified based on experimental results.
DOI: 10.1061/(ASCE)GM.1943-5622.0000534.

Author keywords: Constitutive modeling; Critical state; Bounding surface plasticity; Radial mapping; Cemented sand.

Introduction

Imam (1999) and Imam et al. (2005) developed a critical state constitutive model capable of capturing the response of cohesionless sands. To model artificially or naturally cemented sand, the model requires some modifications to consider the effect of cementations. Cemented soils have a structure that has important effects on their mechanical responses (Yu et al. 2007). The structure in natural soils is believed to be a combination of fabric and bonding, which can be destroyed by plastic deformation (Yu et al. 2007; Yang et al. 2011). Bonding in a general sense includes all types of cohesive forces at the interparticle level by cementing agents (Lee et al. 2004).

Other models have been developed for uncemented and structured sands, such as the disturbed state concept (DSC) (Desai 2000; Liu et al. 2000). In the DSC, continuum deformation is divided into two reference states: the virgin state, or relative intact state, and the disturbed state, or fully adjusted (FA) state. The FA state is often taken to the critical state for sands (Desai and Wang 2003). Disturbance is evaluated using the disturbance degree (D). A disturbed function is used to predict the change of the disturbance with influential factors (for example, plastic deformation).

Because bonding between soil particles gives rise to an increase in stiffness and strength, the initial yield surface is expected to enlarge. This has been supported by experimental observations. However, regardless of the sources of cementation, the engineering effects of the factors due to cementation are similar because they all result in increased stiffness and the development of higher cohesion and tensile strength (Lee et al. 2004). This is why many new models for cemented geomaterials assume a larger yield surface compared with the corresponding uncemented materials (Gens and Nova 1993; Nova et al. 2003; Nova 2006; Navarro et al. 2010). Many models adopt a modified Cam-clay framework because many cemented materials are often clayey in nature. This makes them unsuitable for cemented sands because sand does not have a unique normal consolidation line, which is required in the Cam-clay framework (Jefferies 1993; Yu et al. 2007).

In this new model, cementation is first implemented into the base sand model by incorporating tensile strength and cohesion into the formulation of constitutive relationships. Definitions of the yield function, elastic moduli, plastic-hardening modulus, flow rule, and other components of the model are modified accordingly. After the incorporation of the tensile strength and cohesion into the model, the new model is reformulated using the framework of bounding surface plasticity (Dafalias 1986; Dafalias and Herrmann 1986). By incorporating bounding surface plasticity, the model has the potential of modeling cyclic loading (Imam and Chan 2008).

Bounding surface plasticity was first proposed for metal by Dafalias and Popov (1975). In this theory, stress states are assumed to be bounded by a surface called the bounding surface. Hence, the bounding surface provides an exterior limit for all permissible stress states. It is also assumed that the stress states always lie in another surface called the loading surface. During plastic flow, the bounding surface and loading surface can uniformly expand/contract, move, or even rotate. The bounding surface, however, always contains the current stress state because a stress state outside the bounding surface has no physical meaning. That is, regardless of the size of the loading surface, the bounding surface always encompasses the loading surface. The loading surface may touch the bounding surface tangentially at a point or even become identical with it, but never intersects it. The elastic nucleus is another surface in which the plastic modulus gets an infinite value rather than an explicit value. However, for simplicity, it is usually assumed that the elastic domain diminishes to a single point, meaning the plastic deformation occurs as soon as the loading embarks in the stress space.

The remarkable feature of the bounding-surface concept is that hardening of the loading surface and the resulting magnitude of the plastic deformation depend on the proximity of the stress state to the bounding surface. The loading surface becomes a reference surface for complex stress paths of plastic deformation. In fact, plastic deformation at any stress point inside the bounding surface is computed by dividing the plastic modulus of the loading surface into two segments: the bounding modulus and the additive plastic modulus. Then, radial mapping is used to evaluate the

[1]Research Assistant, Civil and Environmental Engineering Dept., Univ. of Alberta, Edmonton, AB, Canada T6G 2W2 (corresponding author). E-mail: rahimi2726@gmail.com

[2]Professor, Civil and Environmental Engineering Dept., Univ. of Alberta, Edmonton, AB, Canada T6G 2W2; Professor, China Three Gorges Univ., Yichang, China. E-mail: dave.chan@ualberta.ca

[3]Associate Professor, Civil and Environmental Engineering Dept., Univ. of Alberta, Edmonton, AB, Canada T6G 2W2. E-mail: anouri@ualberta.ca

Note. This manuscript was submitted on April 13, 2014; approved on April 7, 2015; published online on June 30, 2015. Discussion period open until November 30, 2015; separate discussions must be submitted for individual papers. This paper is part of the ***International Journal of Geomechanics***, © ASCE, ISSN 1532-3641/04015049(11)/$25.00.

corresponding unique image stress point on the bounding surface needed to calculate these two moduli (Reilly and Brown 1991).

Description of the Base Model

The theory and formulation of the base model can be found in Imam et al. (2005). In this model, the yield function is expressed as

$$f = (\eta - \alpha)^2 - M_\alpha^2\left(1 - \sqrt{\frac{p}{p_c}}\right) = 0 \tag{1}$$

$$M_\alpha^2 = (5M_p - \alpha)(M_p - \alpha) \tag{2}$$

where η = stress ratio; p = mean effective normal stress; α = scalar constant whose magnitude is zero for isotropically consolidated sands; and p_c = effective preconsolidation pressure, which is a hardening parameter controlling the size of the yield surface.

The value of M_p is evaluated for compression and extension, respectively, using the following equations:

$$M_{p,c} = \frac{6\ \sin\varphi_{p,c}}{3 - \sin\varphi_{p,c}} \tag{3}$$

$$M_{p,e} = \frac{6\ \sin\varphi_{p,e}}{3 + \sin\varphi_{p,e}} \tag{4}$$

in which $\varphi_{p,c}$ and $\varphi_{p,e}$ = friction angles at peak shear stress in triaxial compression and triaxial extension, respectively. They are calculated by

$$\sin\varphi_{p,c} = \sin\varphi_\mu - k_p\psi_p \tag{5}$$

$$\sin\varphi_{p,e} = \sin\varphi_\mu - k_p\psi_p - a_p \tag{6}$$

where $\psi_p = e - e_p$, in which e = void ratio and e_p = is the critical state void ratio, which is evaluated at mean normal pressure corresponding to the peak point of shear stress (i.e., at $p = p_p$); φ_μ = friction angle associated with $\psi_p = 0$ in triaxial compression and is usually close to the interparticle friction angle; and k_p and a_p = model parameters.

Similar to conventional plasticity, isotropic elasticity is represented by two elastic parameters: the bulk modulus and shear modulus. They are expressed as a direct function of the mean effective stress and inverse function of the void ratio as follows:

$$G = G_a\frac{(2.973 - e)^2}{1 + e}\left(\frac{p}{p_a}\right)^n \tag{7}$$

$$K = K_a\frac{(2.973 - e)^2}{1 + e}\left(\frac{p}{p_a}\right)^n \tag{8}$$

where G_a and K_a = reference elastic moduli considered as material parameters; and p_a = atmospheric pressure. A value of 0.5–0.6 is usually used for n, depending on the type of sand.

Following the work of Wood (1990) and Manzari and Dafalias (1997), the stress–dilatancy relationship is defined as

$$d = \frac{\dot{\varepsilon}_p^p}{\dot{\varepsilon}_q^p} = A(M_{PT} - \eta) \tag{9}$$

$$A_c = \frac{9}{9 + 3M_{PT,c} - 2M_{PT,c}\eta} \tag{10}$$

$$A_e = \frac{9}{9 - 3M_{PT,c} - 2M_{PT,c}\eta} \tag{11}$$

where

$$\sin\varphi_{PT,c} = \sin\varphi_{cs} + k_{PT}\psi \tag{12}$$

$$\sin\varphi_{PT,e} = \sin\varphi_{cs} + k_{PT}\psi + a_{PT} \tag{13}$$

in which M_{PT} = phase transformation stress ratio when volumetric–plastic strain (and, as a result, dilatancy) changes its sign, resulting in a change in the sign of $\dot{p}$; φ_{cs} = critical state friction angle (a model parameter); $\psi = e - e_{cs}$ = state parameter representing the difference between the current void ratio and the critical state void ratio at the current mean normal stress (Been and Jefferies 1985; Jefferies 1993); and k_{PT} and a_{PT} = material parameters. The phase transformation stress ratio for compression ($M_{PT,c}$) and extension ($M_{PT,e}$) is obtained using $\sin\varphi_{PT,c}$ and $\sin\varphi_{PT,e}$ similarly as for $M_{p,c}$ and $M_{p,e}$. Because of the dependency of M_{PT} on the state parameter, the effect of the void ratio and mean normal effective pressure is indirectly included in the flow rule. Compression and extension behavior are different, and appropriate laboratory tests should be conducted to determine the parameters (Desai 2007).

Hardening in this model depends on the proximity to the critical state, in contrast to conventional critical state models that couple the size of the yield surface to the void ratio and obtain a hardening law based on plastic volumetric strain using a constant p stress path (Schofield 1993; Wood 1990; Bardet 1986; Yu 2006; Yu et al. 2007; Suebsuk et al. 2010, 2011). This is similar to Jefferies's approach (1993), which formulates the size of hardening as a function of the difference between the current maximum hardness and the current size of the yield surface.

The pure shear hardening law is expressed as

$$\frac{\partial p_c}{\partial \varepsilon_q^p} = \frac{hG_{ini}}{(p_f - p_c)_{ini}}(p_f - p_c) \tag{14}$$

in which h = model parameter; p_f = failure mean normal effective stress, which is obtained by substituting the failure stress ratio (M_f) for η in the yield function equation; and $(p_f - p_c)_{ini}$ = initial value of $(p_f - p_c)$ at the end of consolidation and prior to shearing. The value of M_f is calculated using $\sin\varphi_f$, which itself is obtained by adopting a Mohr–Coulomb-type failure criterion as follows:

$$\sin\varphi_f = \sin\varphi_{cs} - k_f\psi \tag{15}$$

where k_f = model parameter. The value of M_f = maximum attainable stress ratio at the current stress state.

Critical State Framework for Bonded Sand

Modification of the base model is carried out using experimental observations that show the differences between the response of cemented/bonded and equivalent uncemented/unbonded soils. Fig. 1 schematically represents the effect of bonding on the isotropic compression curve. It is seen that bonded geomaterials exist at a higher void ratio for the same mean normal pressure, leading to broader admissible states compared with unbonded materials. Differences in the void ratios of bonded and equivalent unbonded materials at their loosest possible state under a specific mean pressure can signify the degree of bonding. As shown in Fig. 1, the degree of bonding may also be taken into account as the difference between the mean normal stresses at the loosest possible state for the bonded and unbonded material under the same void ratio (Vatsala et al. 2001).

Fig. 2, obtained from experiments, exemplifies that the yield (mean effective) stress increases with an increase in cement contents,

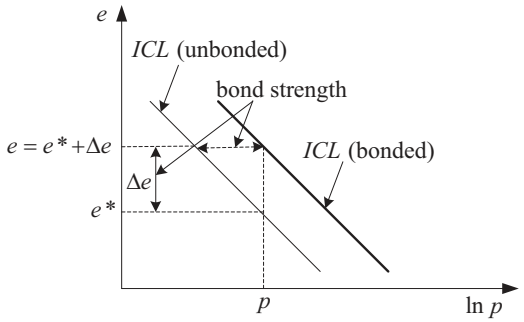

Fig. 1. Idealized representation of compression response for bonded soil

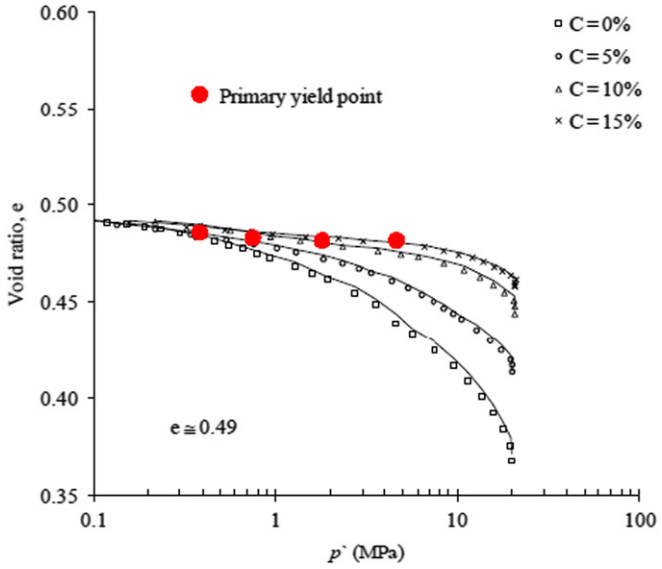

Fig. 2. Effect of cement content on the initial yield point of cement-treated Portaway sand (adapted from Marri 2010, with permission)

implying a larger size for the initial yield surface. Initial yielding is considered as the point at which breakage of the cement bonds commences and is regarded as a state where the compression plane and stress–strain curves deviate from the initial linear response.

Fig. 3 suggests that by increasing the cement contents, there is an increase in the normalized initial yield stress (and peak stress). The position of the yield point also shifts toward the left, implying a stiffer response with an increase in the cement content. It is clear that the tendency for a brittle response under the same confining stress increases with cement content. In an ideal case, the shear stress–strain curve for structured soils will ultimately be identical to that for remoulded soils at a critical state when all cemented bonds have been destroyed. This, however, does not always materialize because some bonds may not be broken, even after an appreciable amount of shearing occurs well beyond the initial yield point (Lee et al. 2004). That is, cemented soil may arrive at the ultimate void ratio after a large amount of shearing rather than at the critical state void ratio, which is associated with constant volume and is independent of the initial state. This is one of the existing challenges in applying the critical state theory in cemented soil, especially in cemented sand. Thus, the CSL may be expected to depend on the initial void ratio for cemented sand, as observed experimentally by Marri (2010). The application of a nonunique CSL has been reported for cohesionless sand, as well. For example, in Bardet's work (1986), different critical state lines are used to calibrate the response of loose and dense Sacramento River sand.

In considering the additional strength, the yield surface for the unbonded geomaterials must be enlarged toward the right. It must also be expanded toward the left to account for the cohesion/tensile strength.

Fig. 4(a) illustrates the schematic of the modified yield surface and the representation in three-dimensional (3D) stress space is shown in Fig. 4(b). For simplicity, the original shape of the yield function is preserved. Expansion toward the right and left are indicated by p_o and p_t, respectively. The value of p_b controls the yielding of the bonded material in isotropic compression, which governs the size of the enlarged yield surface, whereas p_o controls the growth in size of the initial elastic domain. The degree of bonding may be expressed as p_o/p_c.

The surface is closed in isotropic compression and it is smooth. In fact, the tangent plane of the surface is perpendicular to the

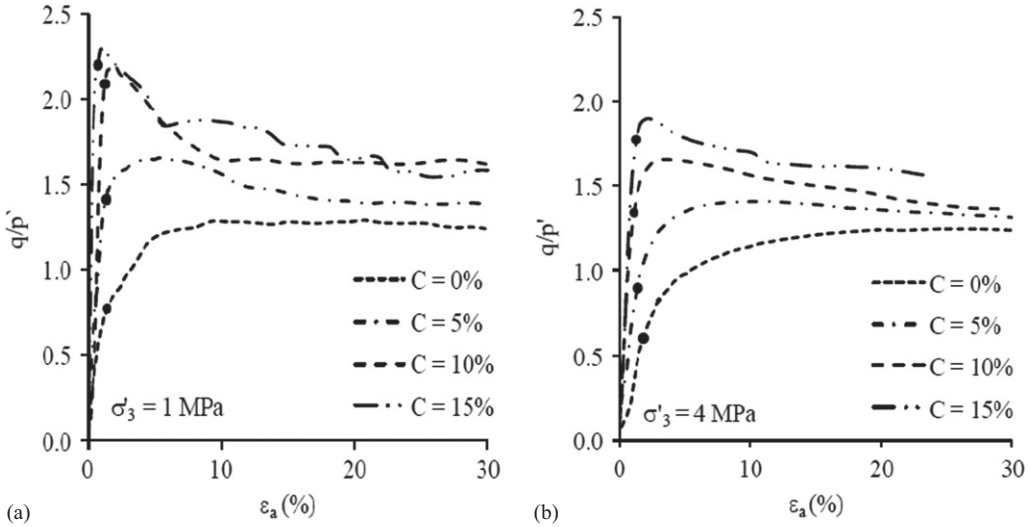

Fig. 3. Effect of cement content on the location of the initial yield point (small bold circles) (reprinted from Marri 2010, with permission): (a) triaxial tests with confining pressure of 1 MPa; (b) triaxial tests with confining pressure of 4 MPa

Int. J. Geomech., 2016, 16(2): 04015049

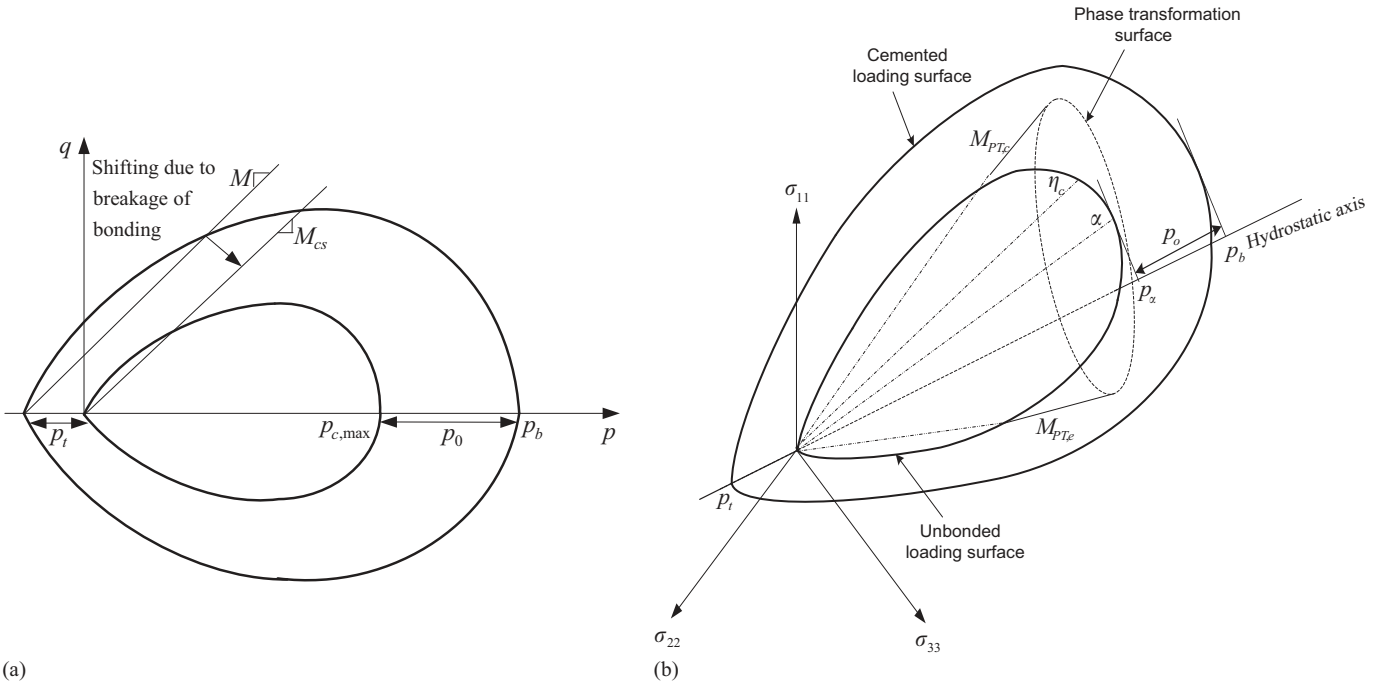

Fig. 4. (a) Schematic of the modified yield surface; (b) representation in 3D stress space of the modified yield surface

p-axis for isotropic material. A singularity point exists under pure tension, that is, shear stress $q = 0$. At this point, the normal surface is different for points approaching from positive q and negative q. In this model, tensile failure is not governed by the plastic flow rule. A tension cutoff scheme is used.

The yield function, flow rule, hardening modulus, and elastic properties are modified to create a new constitutive model suitable for cemented sand. A brief discussion of the modifications for the new constitutive model is presented herein.

Elasticity

On the basis of experimental observations indicating bonded geomaterials have higher stiffness values compared with their reconstituted counterparts (Marri 2010; Yu 2006), the definition of the elastic properties are modified similar to the approach adopted by Yu et al. (2007), as follows:

$$G = G_a \frac{(2.973-e)^2}{1+e}\left[\frac{p}{p_a}\left(1+\sqrt{\frac{p_o}{p}}\right)\right]^n \tag{16}$$

$$K = K_a \frac{(2.973-e)^2}{1+e}\left[\frac{p}{p_a}\left(1+\sqrt{\frac{p_o}{p}}\right)\right]^n \tag{17}$$

Yield Function

$$f = \left(\frac{q}{p+p_t}-\alpha\right)^2 - M_\alpha^2\left(1-\sqrt{\frac{p+p_t}{p_b}}\right) = 0 \tag{18}$$

$$p_b = p_t + p_c + p_o \tag{19}$$

where α and M_α^2 are defined similar to the definitions given in the base model. For triaxial conditions, $\alpha = 0$ and $M_\alpha^2 = 5M_p^2$. The original yield function has been modified according to Gens and Nova (1993). Similar assumptions have also been considered for the relationships between additional strengths and p_c:

$$\frac{p_o}{p_c} = b \tag{20}$$

$$\frac{p_t}{p_c} = \beta b \tag{21}$$

These assumptions suggest a direct relationship between two additional strengths, as follows:

$$p_t = \beta p_o \tag{22}$$

Hence, p_b consists of two components:

$$p_b = p_c + (1+\beta)p_o \tag{23}$$

where p_c plays the same role as the maximum preconsolidation pressure for uncemented soil.

When considering the destruction of bonds, the following simple linear relationship is assumed:

$$dp_o = -\gamma p_o d\left|\varepsilon_q^p\right| \tag{24}$$

Flow Rule

Rowe derived the stress dilatancy relationship for soils using the minimum energy consideration for particle sliding (cited in Imam 1999), as follows:

$$R = KD \quad \text{for TC} \tag{25}$$

$$R = \frac{K}{D} \quad \text{for TE} \tag{26}$$

where $R =$ ratio of the major principal stress to the minor principal stress; $K =$ material parameter; TC = triaxial compression; TE = triaxial extension; and $D =$ dilatancy parameter written using increments of volumetric and major principal strains. The constant K is based on the assumption that the ratio of work done

by the driving stress to the work done by the driven stress in any strain increment should be a constant. Driving and driven stresses for triaxial compression, respectively, are axial and radial stresses. That is, for triaxial compression (Wood 1990)

$$\frac{\sigma_a \dot{\varepsilon}_a}{-2\sigma_r \dot{\varepsilon}_r} = K = \frac{1+\sin\varphi_f}{1-\sin\varphi_f} \tag{27}$$

R, K, and D mathematically are expressed as follows:

$$R = \frac{\sigma_1}{\sigma_3} \tag{28}$$

$$K = \tan^2\left(45+\frac{\varphi_f}{2}\right) \quad \varphi_\mu < \varphi_f < \varphi_{cv} \tag{29}$$

$$D = 1 - \frac{d\varepsilon_v}{d\varepsilon_1} \tag{30}$$

Incorporation of varying φ_f in the constitutive model is difficult (Imam 1999), as φ_f varies between interparticle-friction and critical state friction angles. Thus, a constant value is assumed for φ_f. Assuming a constant value for φ_f (which means a constant volume or critical state friction angle) and neglecting elastic strains, Wood formulated Rowe's stress–dilatancy relationship for the compression and extension of soils, respectively, as follows (Wood 1990):

$$d = \frac{\dot{\varepsilon}_p^p}{\dot{\varepsilon}_q^p} = \frac{9(M_{cs,c}-\eta)}{9+3M_{cs,c}-2M_{cs,c}\eta} \tag{31}$$

$$d = \frac{\dot{\varepsilon}_p^p}{\dot{\varepsilon}_q^p} = \frac{9(M_{cs,e}-\eta)}{9-3M_{cs,e}-2M_{cs,e}\eta} \tag{32}$$

Rowe's relationship, however, does not capture the stress–dilatancy behavior of cemented sand. The deviation of predictions from observed volumetric behavior in some cases become very pronounced, although one may arrive at better predictions for the shear stress–strain curve.

The change in volumetric behavior in the cemented soil mainly depends on the cementation and breakage of particle bonding (Lee et al. 2004). Laboratory test results have suggested that dilatancy is not only affected by the friction angle φ_f, but also by interparticle cohesion. Also, it is believed that the total work performed by the stresses is dissipated partly through friction and partly through destroying the structure. Thus, it is logical to incorporate cohesion into the dilatancy relationship. One approach is by changing the parameter K as follows (Yu et al. 2007):

$$K = \tan^2\left(45+\frac{\varphi_f}{2}\right) + \frac{2c}{\sigma_3}\tan\left(45+\frac{\varphi_f}{2}\right) \tag{33}$$

Normalizing cohesion with respect to the minor principal stress implies that cohesion decreases with an increase in the minor principal stress. This is compatible with experimental observations where the response of bonded materials under triaxial compression change from brittle to ductile with an increase in the confining stress. Crushing of the particles may be one reason for this shift. Even though some experimental evidence suggests the suppression of dilatancy by cohesion (Yu et al. 2007), counter observations regarding the impact of bonding on stress–dilatancy have been reported, as well. For instance, Clough et al. (1981), Asghari et al. (2003), and Marri (2010) found that an increase in the cement contents had a tendency of inducing dilatancy and subsequently reduced compression. According to Fernandez and Santamarina (2000), cemented sand seems to be more dilative than its reconstituted counterpart. Higher dilation under undrained conditions implies that lower excess pore-water pressure is produced by shear, and sand is also less prone to liquefaction. This suggests that bonding enhances the liquefaction resistance of sand (Gao and Zhao 2012). What is clear, however, is that dilatancy is influenced by bonding. The stress–dilatancy relationship, by incorporating cohesion for compression, may be calculated by (Yu et al. 2007)

$$d = \frac{9(M_{cs}-\eta)+6\frac{c}{p}\sqrt{(2M_{cs}+3)(-M_{cs}+3)}}{9+3M_{cs}-2M_{cs}\eta+4\frac{c}{p}\sqrt{(2M_{cs}+3)(-M_{cs}+3)}} \tag{34}$$

Cohesion is assumed to decrease with plastic shear strain, as follows:

$$dc = ce^{-\xi d\left|\varepsilon_q^p\right|} \tag{35}$$

Compatible with Imam's approach (Imam et al. 2005), the dilatancy relationship is written in terms of the variable phase transformation stress ratio rather than the constant critical state stress ratio. For triaxial compression conditions

$$d = \sqrt{\frac{2}{3}}\left[A(M_{PT}-\eta)+\frac{6B}{C}\right] \tag{36}$$

$$A = \frac{9}{C} \tag{37}$$

$$C = 9+3M_{PT,c}-2M_{PT,c}\eta+4B \tag{38}$$

$$B = \frac{c}{p}\sqrt{(2M_{PT}+3)(-M_{PT}+3)} \tag{39}$$

Hardening Modulus

A pure size shear–hardening law is adopted for the modified model. Similar to the base model, shape hardening due to variations of M_p is neglected in the modified model. After some manipulation, and that ensuring the state of stress remains on the modified yield surface, the following formula is derived for the normalized hardening modulus under triaxial conditions:

$$H_n = -\sqrt{\frac{2}{3}}\frac{1}{\left|\frac{\partial f}{\partial q}\right|}\frac{\partial f}{\partial p_b}\frac{\partial p_b}{\partial \varepsilon_q^p} \tag{40}$$

where

$$\frac{\partial f}{\partial p_b} = -\frac{M_\alpha^2}{2p_b}\sqrt{\frac{p+p_t}{p_b}} \tag{41}$$

$$\frac{\partial f}{\partial q} = \frac{2}{p+p_t}\left(\frac{q}{p+p_t}-\alpha\right) \tag{42}$$

$$\frac{\partial p_b}{\partial \varepsilon_q^p} = \frac{\partial p_c}{\partial \varepsilon_q^p}+(1+\beta)\frac{\partial p_o}{\partial \varepsilon_q^p} = \frac{hG_{ini}}{(p_f-p_c)_{ini}}(p_f-p_c)-(1+\beta)\gamma p_o \tag{43}$$

$$\frac{\partial f}{\partial p} = \frac{-2q}{(p+p_t)^2}\left(\frac{q}{p+p_t}-\alpha\right)+\frac{1}{2}M_\alpha^2\frac{1}{\sqrt{p_b(p+p_t)}} \tag{44}$$

$$p_f = \frac{p}{\left[1-\frac{(M_f-\alpha)^2}{M_\alpha^2}\right]^2} \tag{45}$$

Consistent with Gens and Nova (1993), the plastic-hardening modulus is calculated from two competing terms. That is, the variation of the bonded yield surface is controlled by two different mechanisms: (1) an unbounded hardening law, hardening/softening

the unbonded yield surface due to void ratio reduction/augmentation; and (2) bond degradation, shrinking the bonded yield surface by virtue of plastic deformation. Thus, softening occurs when the resultant sign of the plastic modulus becomes negative.

Material Parameters

Five additional model parameters have been introduced in the bonded model:

1. Initial value of p_o,
2. Initial value of tensile strength to evaluate β,
3. Decay parameter of bond strength (γ),
4. Cohesion (c), and
5. Rate of degradation of cohesion (ξ).

The initial value of p_o is equal to the difference between the initial values of p_b and p_c. The initial value of p_c for the triaxial test is taken as the maximum mean normal stress characterizing the initial elastic domain for uncemented soil. The initial value of p_b can be evaluated by conducting an isotropic compression test on soft rock to determine the initial yield value of p_b (Nova 2005).

The parameter β, which controls the size of the tensile strength surface, is obtained when the initial value of the tensile strength is evaluated using results from a tensile test. If there is no data regarding the tensile strength, the unconfined compressive strength may be considered as an approximation for the tensile strength (tensile strength is in the range of 5–20% of the unconfined compressive strength); otherwise, a typical value in the range of 0.05–0.25 may be selected as a value for β.

The parameter γ controls the rate at which bonds are broken. It can only be determined by fitting the theoretical outcomes to the experimental data. The higher value of γ, the faster the bonded yield surface becomes identical to the unbonded yield surface.

The parameter c can be evaluated using the bonded yield function or Mohr–Coulomb yield function.

The parameter ξ can be evaluated by fitting theoretical results to measured experimental data.

If a zero value is assigned for all five additional material parameters, the base model will be recovered.

Bounding Surface Model for Cemented Sand

Elasticity and Flow Rule

For simplicity, all assumptions made for the elasticity and flow rule of the modified bonded model are retained here and remain unchanged.

Bounding and Loading Surfaces

The cemented bounding and loading surfaces in terms of conventional triaxial variables are written as follows:

$$F_{\mathrm{CBS}} = \left(\frac{\overline{q}}{\overline{p}+p_t}-\alpha\right)^2 - M_\alpha^2\left(1-\sqrt{\frac{\overline{p}+p_t}{\overline{p}_b}}\right) = 0 \tag{46}$$

$$F_{\mathrm{CLS}} = \left(\frac{q}{p+p_t}-\alpha\right)^2 - M_\alpha^2\left(1-\sqrt{\frac{p+p_t}{p_b}}\right) = 0 \tag{47}$$

in which

$$\overline{p}_b = p_t + \overline{p}_c + \overline{p}_o \tag{48}$$

$$p_t = \overline{\beta}\overline{p}_o = \beta p_o \tag{49}$$

The superimposed bar signifies variables of the bounding surface.

The relationship of the tensile strength suggests that $\overline{\beta}$ and $\overline{p}_o$ cannot both be chosen arbitrarily because they must result in the same tensile strength obtained from β and p_o. This means only one of them, for instance $\overline{p}_o$, can be chosen as a material parameter. To avoid having more model parameters, $\overline{p}_o$ may be obliged to obtain an initial value that produces the same initial bonding for the cemented bounding surface than that for the cemented loading surface. From this simplifying assumption, it can be shown that

$$\overline{\beta} = \frac{\beta p_o}{\left(\frac{p_o}{p_c}\right)\overline{p}_c} = \frac{\beta p_c}{\overline{p}_c} \tag{50}$$

Thus,

$$\overline{p}_b = \overline{p}_c + \beta\left(1+\frac{1}{\overline{\beta}}\right)p_o \tag{51}$$

The initial values of p_c and $\overline{p}_c$ are evaluated from the confining pressure and failure mean normal pressure at the commencement of shearing, respectively. Fig. 5 illustrates the proposed bounding surface model, where LS, CLS, BS, and CBS, respectively, stand for loading surface, cemented loading surface, bounding surface (which is associated with loading surface), and cemented bounding surface (associated with cemented loading surface).

For simplicity, the size ratio between the cemented loading and cemented bounding surfaces is assumed to remain fixed in the course of plastic loading. The application of a fixed size ratio between the loading and bounding surfaces already has been practiced by several researchers (Al-Tabbaa 1987; Hau 2003; McDowell and Hau 2004).

Projection Rule

The radial mapping rule is used to associate any current stress point with a corresponding unique image point. This is achieved by the intersection of the cemented bounding surface with a line

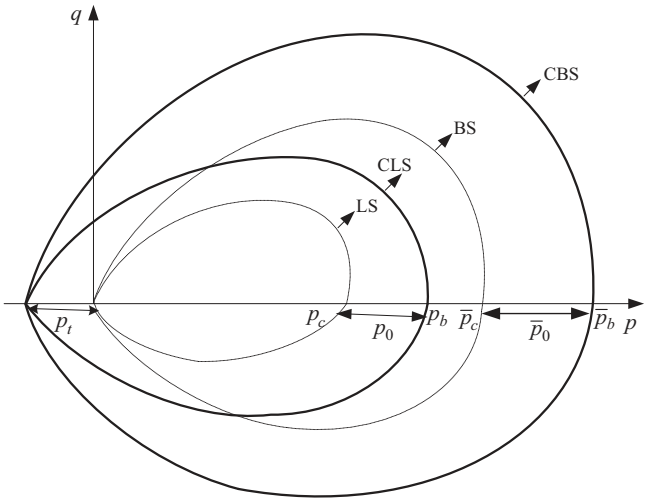

Fig. 5. Schematic representation of the proposed bounding surface model within a conventional triaxial (p, q) space

passing through the projection center and the current stress point (see Fig. 6). Because of the similarity in shape and radial symmetry of the surfaces, the unique image stresses ($\overline{p}$, $\overline{q}$) can be evaluated using the current stresses (p, q) as follows:

$$\frac{\overline{p}+p_t}{p+p_t}=\frac{\overline{q}}{q}=\frac{\overline{p}_b}{p_b}=b \quad 1\le b\le\infty \tag{52}$$

Because the projection center is not at the origin of the coordinate system, stress ratios at the current stress point and the corresponding image point are not the same. However, they are equal at the limiting state when all structures have been destroyed (i.e., tensile strength reduces to zero).

The mapping rule is not invertible (i.e., although a unique image stress exists on the bounding surface for a given current stress on the loading surface, a given image stress may correspond to many stress states (Dafalias 1986).

Hardening Modulus

In line with the mainstream approach for bounding surface plasticity, the plastic-hardening modulus is divided into two parts: the bounding surface modulus and the additive plastic modulus.

$$H_n=\overline{H}_n+H_f \tag{53}$$

The additive plastic modulus indicates a dependency of the response on the relative distance between the current stress point and corresponding image point. The dependency of the plastic response on the distance between the current stress and its image point stemmed from experimental observations where uniaxial stress–strain curves asymptotically approached fixed or variable bounds in the stress space under complex loading histories (Chen 1994; Chen and Han 2007). The following formula is proposed for the additive plastic modulus:

$$H_f=\frac{\Gamma\cdot p\cdot\delta}{(\delta_o-\delta)^2} \tag{54}$$

The parameter $\Gamma=$ dependency of the response to the type of material; and $\delta=$ distance between the current stress point and the corresponding image point:

$$\delta=\sqrt{(\overline{p}-p)^2+(\overline{q}-q)^2} \tag{55}$$

where δ_o is the initial value of δ.

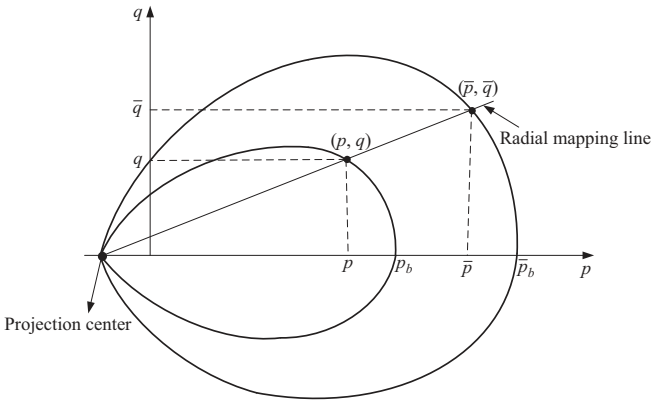

Fig. 6. Radial mapping rule for a conventional triaxial (p, q) space

This definition guarantees that H_f is always positive and has an infinite value at the start of shearing. The value of H_f reduces to zero when the loading surface and bounding surface for the cementation coincide. These are prerequisite for the additive plastic modulus definition (Vermeer and de Borst 1984).

The value of $\overline{H}_n$ is calculated by coercing the state of stress to remain on the bounding surface for a special case when two surfaces coincide. Under triaxial conditions, it can be shown that

$$\overline{H}_n=-\sqrt{\frac{2}{3}}\frac{1}{\left|\frac{\partial F}{\partial\overline{q}}\right|}\frac{\partial F}{\partial\overline{p}_b}\frac{\partial\overline{p}_b}{\partial\varepsilon_q^p} \tag{56}$$

in which

$$\frac{\partial F}{\partial\overline{p}_b}=-\frac{M_\alpha^2}{2\overline{p}_b}\sqrt{\frac{\overline{p}+p_t}{\overline{p}_b}} \tag{57}$$

$$\frac{\partial F}{\partial\overline{q}}=\frac{2}{\overline{p}+p_t}\left(\frac{\overline{q}}{\overline{p}+p_t}-\alpha\right) \tag{58}$$

$$\frac{\partial\overline{p}_b}{\partial\varepsilon_q^p}=\frac{\partial\overline{p}_c}{\partial\varepsilon_q^p}+\beta\left(1+\frac{1}{\overline{\beta}}\right)\frac{\partial p_o}{\partial\varepsilon_q^p} \tag{59}$$

$$\frac{\partial\overline{p}_c}{\partial\varepsilon_q^p}=\frac{hG_{ini}}{\left(\overline{p}_f-\overline{p}_c\right)_{ini}}\left(\overline{p}_f-\overline{p}_c\right) \tag{60}$$

It is assumed that linear destruction of the structure by plastic shear deformation gives rise to changes in the size of the cemented loading surface. Its shape, however, is supposed to remain unchanged because of this destruction. That is

$$\frac{\partial p_o}{\partial\varepsilon_q^p}=-\gamma p_o \tag{61}$$

With the application of six additional model constants, the base model is modified to replicate the response of cemented sands using bounding surface plasticity.

Assessment of the Proposed Bounding Surface Model

The proposed bounding-surface model is evaluated against the drained triaxial compression tests of two artificially cemented sands under different void ratios and confining pressures. The first set of experimental observations comes from the observed behavior of artificially cemented Ottawa sand (Wang and Leung 2008). Figs. 7–9 compare the simulated and measured response of cemented Ottawa sand for different cement contents in terms of shear stress–strain, void ratio–axial strain, and volumetric strain–axial strain plots. Table 1 lists the model parameters for Ottawa cemented sand with 1% cement content. The same material parameters are used also for prediction of behavior of 2 and 3% cement content samples, excluding critical state friction angle, critical state line, and cohesion. Experimentally measured cohesion and critical state friction angles of 11.5 kPa and 30.9° were used for 2% cement content samples, whereas values of 44 kPa and 31.1° were used for 3% cement content samples. The following ultimate state lines were also adopted for 2 and 3% cement content samples:

$$e_{cs}(2\%)=-0.00635p^{*3}+0.03670p^{*2}-0.11991p^*+0.790(p^*\text{ in MPa})$$

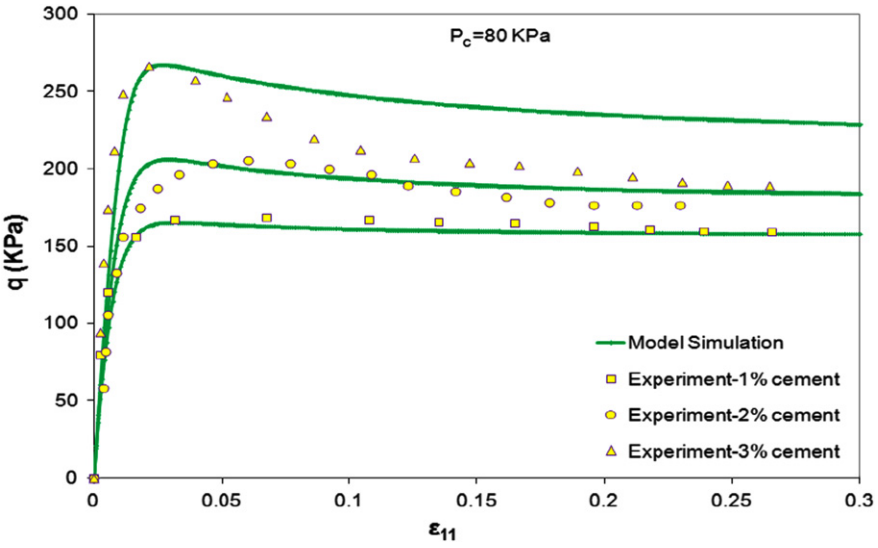

Fig. 7. Measured and predicted response of cemented Ottawa sand for deviator stress versus axial strain curve under different cement contents

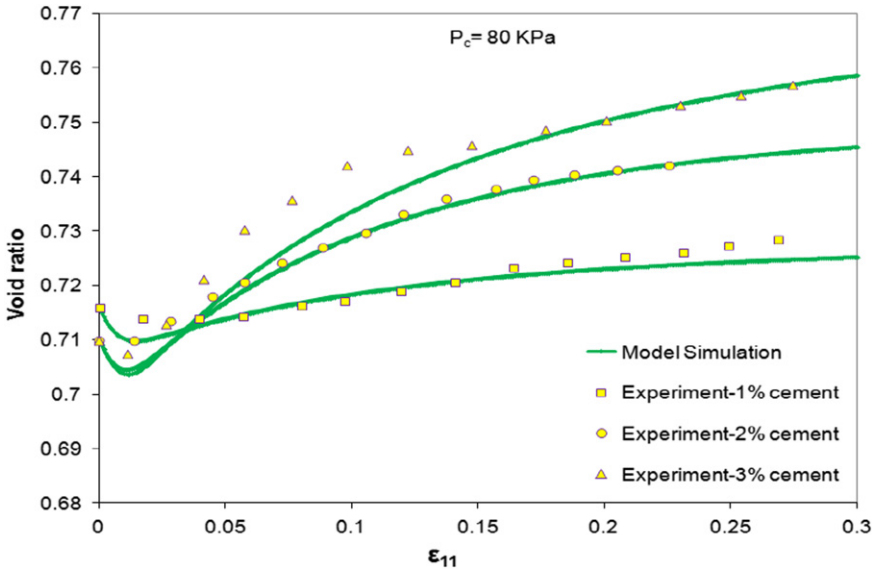

Fig. 8. Measured and predicted response of cemented Ottawa sand for void ratio versus axial strain curve under different cement contents

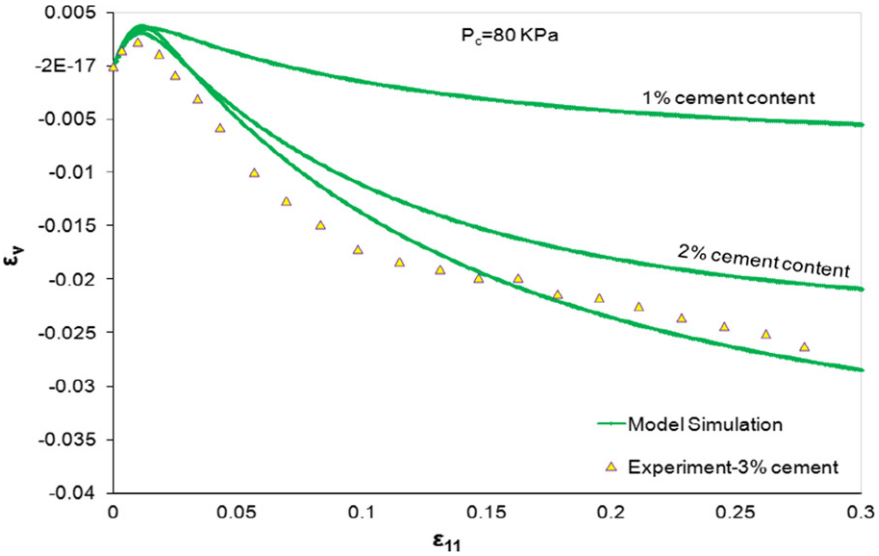

Fig. 9. Measured and predicted response of cemented Ottawa sand for volumetric strain versus axial strain curve under different cement contents

$$e_{cs}(3\%) = -0.00635p^{*3} + 0.03670p^{*2} - 0.11991p^* + 0.8725(p^* \text{ in MPa})$$

It is believed that after a large shear-induced volume change, cohesionless sand ultimately arrives at a unique void ratio independent of its initial state (initial void ratio and confining pressure). This unique void ratio is associated with the complete destruction of the soil structure and a theoretically infinite amount of shearing. Fig. 8, however, reveals a noteworthy point for the ultimate state of the same cemented sand with different cement contents. It is clear that samples with different cement content arrive at different ultimate void ratios after an appreciable amount of shearing. This implies there is no unparallel critical state line that forms the ultimate state for all distortional processes. That is, CSL depends on cement content. It also can be inferred that the CSL for higher cement contents lies at a high position in the compression plane ($e - \ln p$) because it gives rise to a higher ultimate void ratio at a given confining pressure. These observations are confirmed by the computed ultimate void ratios for cemented Portaway sand.

Table 1. Material Parameters Used for Calibration of Cemented Ottawa Sand (1%), $p^* = p + p_t$

Parameter name	Ottawa cemented sand (1%)
k_p	1.5
φ_μ	20
φ_{cs}	28.8
k_{PT}	1.4
G_a	6×10^6
K_a	8×10^6
h	1
k_f	0.75
e_{cs}	$-0.00635\,p^{*3} + 0.03670\,p^{*2} - 0.11991\,p^* + 0.760$ (p^* in MPa)
p_o	0.12×10^6
γ	10
β	0.107
c	0.0075×10^6
ξ	0.08
Γ	1

As seen in Figs. 8–9, the predicted and measured volumetric behaviors are in good agreement. The change of response from contractive to dilative, which is associated with strain softening, is captured in all tests. This change of behavior is predicted numerically by a change of the dilatancy rate sign from positive to negative. This causes an immediate change in the sign of the plastic volumetric strain increment. The sign of the total volumetric strain increment also varies owing to this change after a short time. It is also clear from Figs. 7–9 that samples with higher cement content show stronger dilative and more brittle behavior. There is a small discrepancy in the predicted and observed stress-strain behavior of the test with 3% cement content. That is, the model has predicted weaker softening response for the postpeak region of the test with 3% cement content. It can only approximate the softening postpeak response of the material.

The second set of experimental data was obtained from the observed responses of artificially cemented Portaway sand (Marri 2010). Figs. 10–11 show the simulated and observed behavior of cemented Portaway sand under different cement contents for deviatoric stress–strain and volumetric strain–axial strain curves. Fig. 12 exhibits the predicted response for the void ratio–axial strain curve. Material parameters and their assigned values for the simulation of Portaway cemented sand with a 5% cement content are presented in Table 2. For the 10% cement content test, measured cohesion of 3.18 MPa and critical state friction angle of 36° have been used. The other remaining material parameters for the 10% cement content samples are the same as those used for the 5% cement content samples. For 0% cement content samples, zeros were assigned for all five additional material parameters related to cementation. Except for the critical state line, the other material parameters for the 0% cement content test are the same as the unbounded material parameters for the 5% cement content samples. The following ultimate state lines are adopted based on experimental observations:

$$e_{cs}(10\%) = 0.60 - 0.0097 \ln(p^*)(p^* \text{ in MPa})$$
$$e_{cs}(0\%) = 0.402 - 0.0086 \ln(p^*)(p^* \text{ in MPa})$$

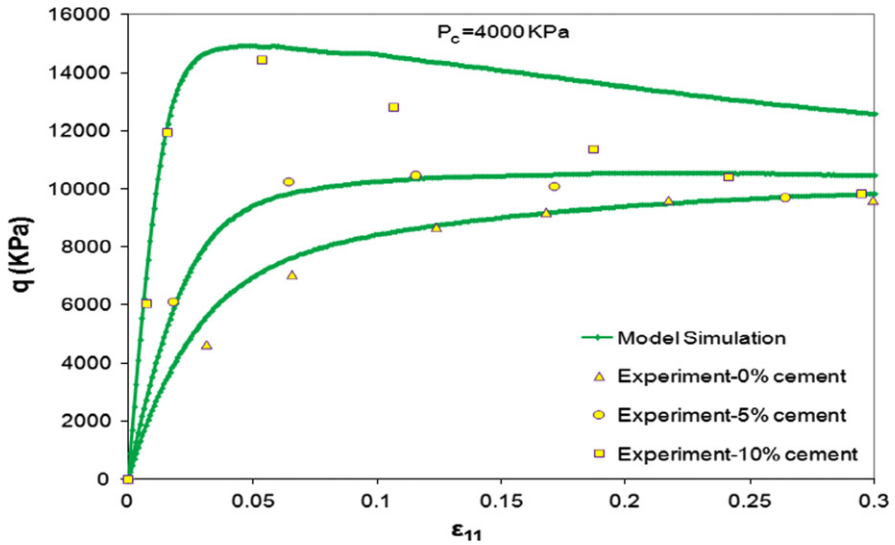

Fig. 10. Measured and predicted response of cemented Portaway sand for deviator stress versus axial strain curve under different cement contents

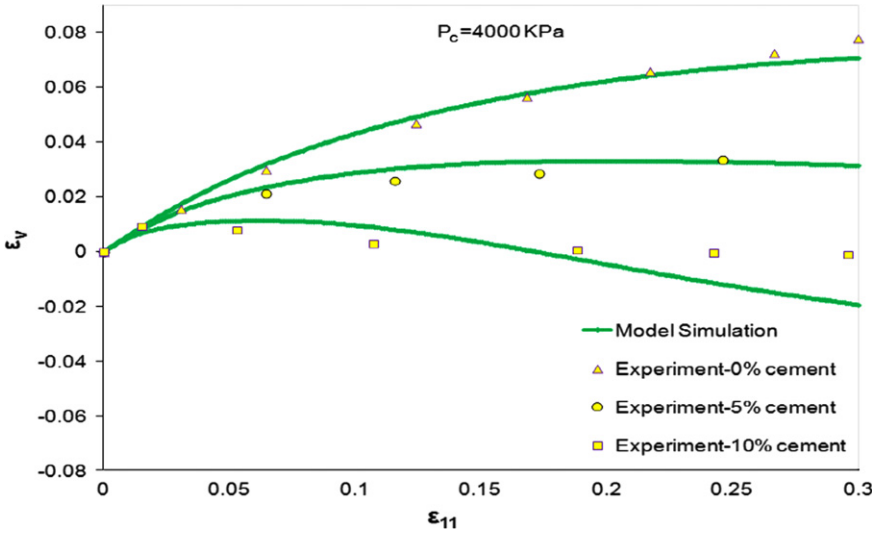

Fig. 11. Measured and predicted response of cemented Portaway sand for volumetric strain versus axial strain curve under different cement contents

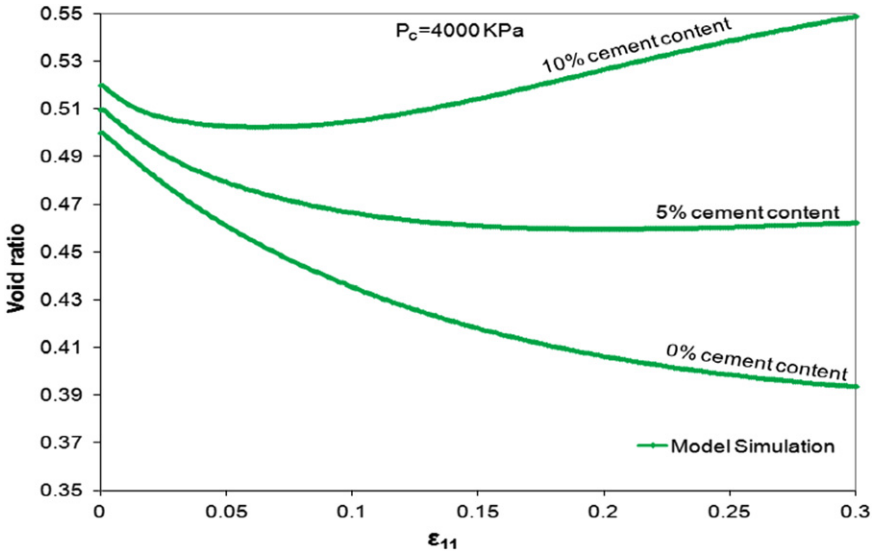

Fig. 12. Predicted response of cemented Portaway sand for void ratio versus axial strain curve under different cement contents

Table 2. Material Parameters Used for Calibration of Artificially Cemented Portaway Sand (5%)

Parameter name	Portaway cemented sand (5%)
k_p	1
φ_μ	32
φ_{cs}	34
k_{PT}	1.25
G_a	10×10^6
K_a	28×10^6
h	1
k_f	0.75
e_{cs}	$0.49 - 0.00925 \ln(p + p_t)$ (p and p_t in MPa)
p_o	8×10^6
γ	5
β	0.10
c	1.08×10^6
ξ	2
Γ	1

Figs. 10–11 show that the proposed model has captured the progressive compressive and ductile behavior of 0 and 5% cement content samples well. The sign of the dilatancy rate and volumetric strain increment remains unchanged throughout shearing for tests with ductile behavior. Though the 5% cement content sample shows compressive response, the tendency for compression is less compared with that of the 0% cement content sample. This decreasing trend for compression is seen in the 10% cement content sample, as well, so that the change of compressive to dilative behavior is observed clearly for the sample with 10% cement content. The model is less accurate in capturing the strain-softening characteristics for 10% cement content. The weaker drop in the peak deviator stress has been predicted by the model for the postpeak region. The selection of an alternative flow rule can improve the prediction of the brittle response. However, defining a reliable stress–dilatancy relationship is a challenging task for cemented soil in general and for cemented sand in particular because it is difficult to simultaneously match both observed volumetric and shear behaviors perfectly for the samples with brittle response.

Conclusion

A bounding surface model for monotonic loading of cemented sands has been presented in this paper. Two sets of triaxial compression tests on artificially cemented sands with different cement contents, void ratios, and confining pressures were chosen to assess the performance of the proposed modified model. In line with the existence of various ultimate void ratios, different critical state lines were selected for the calibration of cemented sands under different cement contents. A comparison of the simulated and observed behaviors shows the model's effectiveness in capturing both the stress–strain behavior and volume change characteristics of cemented material. It is often difficult to capture the bond degradation of cemented material resulting in softening behavior and volume change characteristics. The proposal has its limitation in predicting the strain softening response for material with high cement content.

Acknowledgments

The authors would like to acknowledge the research funding for this study provided by the National Sciences Engineering Research Council of Canada through a Collaborative Research Development program supported by BP Canada.

References

Al-Tabbaa, A. (1987). "Permeability and stress-strain response of speswhite kaolin." Ph.D. thesis, Univ. of Cambridge, Cambridge, U.K.

Asghari, E., Toll, D. G., and Haeri, S. M. (2003). "Triaxial behaviour of a cemented gravely sand, Tehran alluvium." *Geotech. Geol. Eng.*, 21(1), 1–28.

Bardet, J. P. (1986). "Bounding surface plasticity model for sands." *J. Eng. Mech.*, 10.1061/(ASCE)0733-9399(1986)112:11(1198), 1198–1217.

Been, K., and Jefferies, M. G. (1985). "A state parameter for sands." *Géotechnique*, 35(2), 99–112.

Chen, W. F. (1994). *Constitutive equations for engineering materials*, Vol. 2: Plasticity and modeling, Elsevier, New York.

Chen, W. F., and Han D. J. (2007). *Plasticity for structural engineers*, John Ross Publishing, Ft. Lauderdale, FL.

Clough, G. W., Shafii Rad, N., Bachus, R. C., and Sitar, N. (1981). "Cemented sands under static loading." *J. Geotech. Engrg. Div.*, 107(6), 799–817.

Dafalias, Y. F. (1986). "Bounding surface plasticity. I: Mathematical foundation and hypoplasticity." *J. Eng. Mech.*, 10.1061/(ASCE)0733-9399(1986)112:9(966), 966–987.

Dafalias, Y. F., and Herrmann, L. R. (1986). "Bounding surface plasticity. II: Application to isotropic cohesive soils." *J. Eng. Mech.*, 10.1061/(ASCE)0733-9399(1986)112:12(1263), 1263–1291.

Dafalias, Y. F., and Popov, E. P. (1975). "A model of nonlinearly hardening materials for complex loading." *Acta Mech.*, 21(3), 173–192.

Desai, C. S., (2000). "Evaluation of liquefaction using disturbed state and energy approaches." *J. Geotech. Geoenviron. Eng.*, 10.1061/(ASCE)1090-0241(2000)126:7(618), 618–631.

Desai, C. S. (2007). "Unified DSC constitutive model for pavement materials with numerical implementation." *Int. J. Geomech.*, 10.1061/(ASCE)1532-3641(2007)7:2(83), 83–101.

Desai, C. S., and Wang, S. C. (2003). "Disturbed state model for porous saturated materials." *Int. J. Geomech.*, 10.1061/(ASCE)1532-3641(2003)3:2(260), 260–265.

Fernandez, A. L., and Santamarina, J. C. (2000). "Effect of cementation on the small-strain parameters of sands." *Can. Geotech. J.*, 38(1), 191–199.

Gao, Z., and Zhao, J. (2012). "Constitutive modeling of artificially cemented sand by considering fabric anisotropy." *Comput. Geotech.*, 41, 57–69.

Gens, A., and Nova, R. (1993). "Conceptual bases for a constitutive model for bonded soils and weak rocks." *Proc., Symp. on Geotechnical Engineering of Hard Soils–Soft Rocks*, Athens, Greece, Anagnostopoulos et al., 485–494.

Hau, K. W. (2003). "Application of a three surface kinematic hardening model to the repeated loading and thinly surfaced pavements." Ph.D. thesis, Univ. of Nottingham, Nottingham, U.K.

Imam, M. R. (1999). "Modeling the constitutive behavior of sand for the analysis of static liquefaction." Ph.D. thesis, Univ. of Alberta, Edmonton, AB, Canada.

Imam, M. R., and Chan, D. (2008). "Application of a critical state model for the cyclic loading of sands." *Proc., 61th Canadian Geotechnical Conf.*, Edmonton, Canada, 127–134.

Imam, S. M. R., Morgenstern, N. R., Robertson, P. K., and Chan, D. H. (2005). "A critical-state constitutive model for liquefiable sand." *Can. Geotech. J.*, 42(3), 830–855.

Jefferies, M. G. (1993). "Nor-sand: A simple critical state model for sand." *Géotechnique*, 43(1), 91–103.

Lee, K. H., Chan, D. H., and Lam, K. C. (2004). "Constitutive model for cement treated clay in a critical state framework." *Soils Found.*, 44(3), 69–77.

Liu, M. D., Carter, J. P., Desai, C. S., and Xu, K. J. (2000). "Analysis of the compression of structured soils using the disturbed state concept." *Int. J. Numer. Anal. Methods Geomech.*, 24(8), 723–735.

Manzari, M. T., and Dafalias, Y. F. (1997). "A critical state two-surface plasticity model for sands." *Géotechnique*, 47(2), 255–272.

Marri, A. (2010). "The mechanical behaviour of cemented granular materials at high pressures." Ph.D. thesis, Univ. of Nottingham, Nottingham, U.K.

McDowell, G. R., and Hau, K. W. (2004). "A generalised modified cam clay model for clay and sand incorporating kinematic hardening and bounding surface plasticity." *Granular Matter*, 6(1), 11–16.

Navarro, V., Alonso, J., Calvo, B., and Sanchez, J. (2010). "A constitutive model for porous rock including effects of bond strength degradation and partial saturation." *Int. J. Rock Mech. Min. Sci.*, 47(8), 1330–1338.

Nova, R. (2005). "A simple elastoplastic model for soils and soft rocks." *Proc., Soil Constitutive Models: Evaluation, Selection, and Calibration*., ASCE, Reston, VA, 380–399.

Nova, R. (2006). "Modelling of bonded soils with unstable structure." *Springer proceedings in physics: Modern trends in geomechanics*, Vol. 106, Springer, 129–142.

Nova, R., Castellanza, R., and Tamagnini, C. (2003). "A constitutive model for bonded geomaterials subject to mechanical and/or chemical degradation." *Int. J. Numer. Anal. Methods Geomech.*, 27(9), 705–732.

Reilly, M. P. O., and Brown, S. F. (1991). *Cyclic loading of soils: From theory to design*, Blackie and Son Ltd., Glasgow, Scotland, U.K.

Schofield, A. N. (1993). "Original Cam-Clay." *Int. Conf. on Soft Soil Engineering*, Science Press, Guangzhou, China, 40–49.

Suebsuk, J., Horpibulsuk, S., and Liu, M. D. (2010). "Modified structured Cam Clay: A generalised critical state model for destructured, naturally structured and artificially structured clays." *Comput. Geotech.*, 37(7), 956–968.

Suebsuk, J., Horpibulsuk, S., and Liu, M. D. (2011). "A critical state model for overconsolidated structured clays." *Comput. Geotech.*, 38(5), 648–658.

Vatsala, A., Nova, R., and Murthy, B. R. S. (2001). "Elastoplastic model for cemented soils." *J. Geotech. Geoenviron. Eng.*, 10.1061/(ASCE)1090-0241(2001)127:8(679), 679–687.

Vermeer, P. A., and de Borst, R. (1984). "Non-associated plasticity for soils, concrete and rocks." *Heron*, 29(3), 1–64.

Wang, Y. H., and Leung, S. C. (2008). "Characterization of cemented sand by experimental and numerical investigations." *J. Geotech. Geoenviron. Eng.*, 10.1061/(ASCE)1090-0241(2008)134:7(992), 992–1004.

Wood, D. M. (1990). *Soil behavior and critical state soil mechanics*, Cambridge University Press, New York.

Yang, C., Huang, M. S., and Cui, Y. J. (2011). *Constitutive model of unsaturated structured soils under cyclic loading*, Taylor and Francis Group, London, 987–992.

Yu, H. S. (2006). *Plasticity and geotechnics*, Springer, New York.

Yu, H. S., Tan, S. M., and Schnaid, F. (2007). "A critical state framework for modeling bonded geomaterials." *Geomech. Geoeng.*, 2(1), 61–74.